nature photonics

ARTICLES

https://doi.org/10.1038/s41566-020-0636-7

Dynamics of the Berezinskii–Kosterlitz–Thouless transition in a photon fluid

Guohai Situ[1,2,3]✉ and Jason W. Fleischer[1]✉

In addition to enhancing confinement, restricting optical systems to two dimensions gives rise to new photonic states, modified transport and distinct nonlinear effects. Here we explore these properties in combination and experimentally demonstrate a Berezinskii–Kosterlitz–Thouless phase transition in a nonlinear photonic lattice. In this topological transition, vortices are created in pairs and then unbind, changing the dynamics from that of a photonic fluid to that of a plasma-like gas of free (topological) charges. We explicitly measure the number and correlation properties of free vortices, for both repulsive and attractive interactions (the photonic equivalent of ferromagnetic and antiferromagnetic conditions), and confirm the traditional thermodynamics of the Berezinskii–Kosterlitz–Thouless transition. We also suggest a purely fluid interpretation, in which vortices are nucleated by inhomogeneous flow and driven by seeded instability. The results are fundamental to optical hydrodynamics and can impact two-dimensional photonic devices if temperature and interactions are not controlled properly.

Phase transitions give crucial insight into many-body systems, as crossovers between different regimes of order are determined by the underlying dynamics. These dynamics, in turn, are often constrained by dimensionality and geometry. For example, in one-dimensional (1D) and two-dimensional (2D) systems with continuous symmetry, thermal fluctuations prevent the formation of long-range order[1,2]. Two-dimensional systems are distinct, however, as vortices can form in the plane but cannot tilt out of it. At high temperatures, random motion of these vortices destroys large-scale coherence. At low temperatures, vortices with opposite spin can pair together, cancelling their circulation and allowing quasi-long-range order to appear. This Berezinskii–Kosterlitz–Thouless (BKT) transition[3,4] has much in common with Bose–Einstein condensation, which can also occur in two dimensions when the system is bounded[5,6]. Indeed, there is a smooth connection between the two in the limit of vanishing interactions.

To date, experimental evidence for the BKT transition has been obtained only in trapped quantum systems. These span a variety of condensed-matter systems, including superfluids[7], superconductors[8], exciton–polariton systems[9] and cold[6] atoms, across a wide range of temperatures, confining potentials and boundary conditions. Nevertheless, the crossover is essentially classical, and photonic versions of the BKT have been predicted[10–14]. Indeed, photonics systems can support dynamics as rich as their condensed-matter counterparts[15] while being far simpler experimentally, as initial beam profiles can be controlled easily[16], potentials can be induced holographically[17] and the output can be imaged directly. Coherent laser light provides a zero-temperature baseline, so that purely superfluid behaviour can be observed without interference from a normal component[18,19], while thermal features can be controlled by adding a random-phase component to the beam[20]. To date, thermalization[21,22] and condensation of photons[20,23] have been observed, but no evidence for an optical BKT transition has been found. Here we observe all aspects of the BKT transition by considering the nonlinear propagation of a random-phase optical beam.

Results

Model. As in previous work on optical superfluidity, we consider a propagating beam in a nonlinear medium. In the paraxial approximation, the behaviour of the electric field E is given by

$$2ik_0\partial_z E + \nabla_\perp^2 E + 2k_0^2\frac{\Delta n}{n_0}E = 0 \tag{1}$$

where $k_0 = 2\pi n_0/\lambda$ is the wavenumber for a field of wavelength λ, n_0 is the base refractive index and Δn is an index change caused by self-induced (nonlinear) or applied potentials. For the photorefractive crystals used below, the nonlinear response $\Delta n = -\frac{1}{2}n_0^3 r_{ij}E_0 I/(1+sI)$, where $n_0 = 2.3$, r_{ij} is the electro-optic coefficient, E_0 is an electric field bias applied across the crystalline c axis, $I = |E|^2$ is the intensity and s is a parameter describing saturation (for example, due to a finite number of charge carriers). When saturation is negligible, the photorefractive response can be approximated as a cubic Kerr nonlinearity; in this form, equation (1) reduces to

$$i\partial_z A + \nabla_\perp^2 A + \gamma|A|^2 A + V(x)A = 0 \tag{2}$$

where the electric field $E = \sqrt{2/n_0}A$ has been scaled with respect to the base index, the length coordinates (x,y,z) have been scaled with respect to the wavenumber k_0, γ is the strength of the (scaled) nonlinearity and $V(x)$ is an imposed potential ($V = 0$ for the homogeneous system). Equation (2) is known as the nonlinear Schrödinger equation in fluids and optics and the Gross–Pitaevskii equation in condensed matter, with the analogy made complete by considering propagation along the optical axis z as evolution in time, the wavenumber k_0 as an effective mass and the nonlinear term as an effective interparticle (s-wave) interaction.

Equation (2) is a reduced form of the complex Ginzburg–Landau (CGL) equation and inherits many of its properties, including breather solutions, pattern-forming instabilities and phase transitions[24]. In two dimensions (and higher), it also supports vortices.

[1]Department of Electrical Engineering, Princeton University, Princeton, NJ, USA. [2]Shanghai Institute of Optics and Fine Mechanics, Chinese Academy of Sciences, Shanghai, China. [3]Hangzhou Institute for Advanced Study, University of Chinese Academy of Sciences, Hangzhou, China.
✉e-mail: ghsitu@siom.ac.cn; jasonf@Princeton.EDU

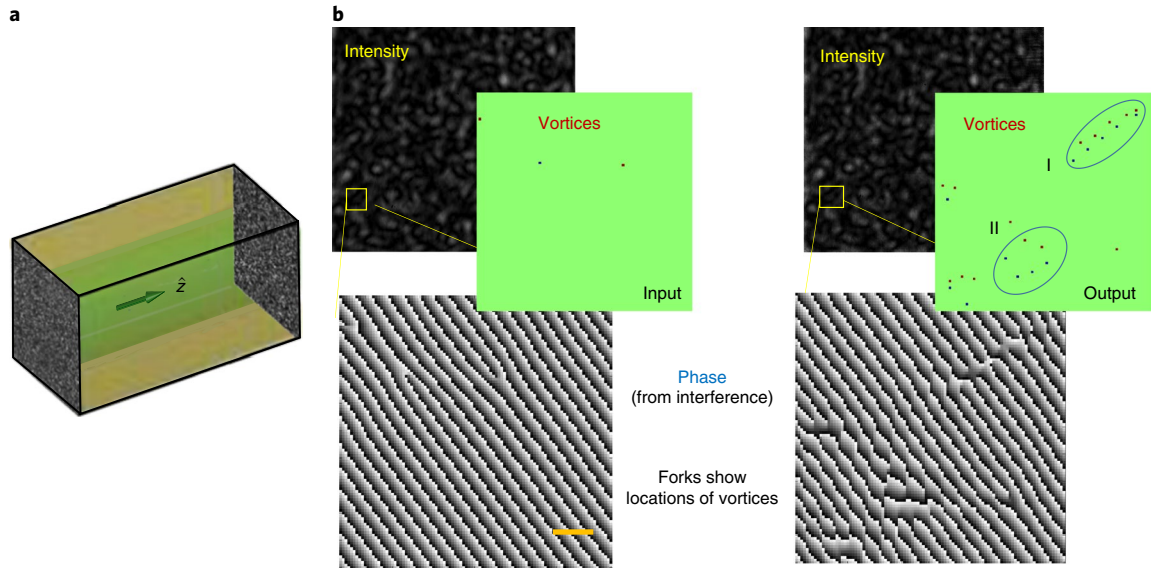

Fig. 1 | BKT transition in a nonlinear optical beam. a, Schematic illustrating the change of a random-phase speckle pattern as it propagates along $\hat{z}$ through a nonlinear crystal. **b**, Experimental results showing typical input and output pictures. Phase profiles, obtained by interfering the waves with a separate reference beam (not shown), show a proliferation of vortices (forks in the phase) above the critical temperature. The green images highlight the locations of the vortices in the phase maps, which were obtained from experimental measurements. The labels highlight sets of bound (I) and free (II) vortices. Scale bar, 100 μm.

Indeed, within photonics, BKT transitions have been predicted in lasers near threshold[10,11] (where the CGL equation describes mean-field dynamics[25]), polariton condensates[13] and nonlinear beams[12,14]. In laser and polariton systems, however, there are difficulties in reaching the CGL regime[26] and in defining a temperature analogue to standard phase transition models. In the latter system, both of these issues are overcome.

In the beam formulation (equation (2)), temperature can be defined even for a single colour by considering the spatial coherence of the beam. Laser light provides a zero-temperature baseline[18], while statistical or random-phase light has an effective temperature given by the full-width at half-maximum (FWHM) of its angular spread[20]. As shown in equations (1) and (2), nonlinearity can reinforce or compete with diffraction (effective kinetic energy), rearranging modes—and thus distributions—through convolution (Fig. 1a). Dynamics experimentally demonstrated from this nonlinear mixing include shock waves[18], instability[19] and wave turbulence[20].

To see explicitly how the BKT transition could arise in the optical system, it is helpful to use a periodic potential $V(x)$ and discretize the diffraction operator. In this (tight-binding) approximation, equation (2) becomes[27]

$$i\mathrm{d}_z A_n = -J\sum_{m(n)} A_m + \gamma|A_n|^2 A_n \tag{3}$$

where d_z is the differential of A_n with respect to z, $A_n = |A_n|\exp[i\phi_n]$ is the complex wavefunction of the mode in the nth lattice site, the phase $\phi_n \in [0, 2\pi)$ corresponds to a localized 'spin', J is the coupling coefficient between nearest neighbours and $\Sigma_{m(n)}$ indicates a sum over adjacent sites. The corresponding Hamiltonian

$$\mathcal{H}(A_n) = -\frac{1}{2}\sum_{<m,n>}\left(A_n A_m^* + A_n^* A_m\right) + \frac{1}{2}|\Gamma|\sum_{n=1}^{N} I_n^2 \tag{4}$$

is characterized by the ratio of self-energy to coupling, $\Gamma = \gamma|A_n|^2/J = \gamma I_n/J$. For strong nonlinearity, the amplitude and phase decouple; in this limit, the angular part $\cos(\phi_m - \phi_n)$ corresponds to the traditional XY model of condensed-matter physics, while the amplitude part $|\Gamma|\sum_{n=1}^{N} I_n^2$ is conserved on its own (in addition to $\mathcal{H}$ as a whole)[28,29]. It is thus possible to define a partition function[28]

$$Z = \int_0^{\infty}\int_0^{2\pi}\prod_m \mathrm{d}\phi_m \mathrm{d}A_m \mathrm{e}^{-\beta(\mathcal{H}+\mu I^2)} \tag{5}$$

where $\beta = 1/T$ and μ define an effective temperature and chemical potential, respectively, in analogy with conventional thermodynamics. The latter ensures the conservation of I^2 and controls the phase transition dynamics of the system, for example, the creation of localized breather states[28,30] or the condensation of waves[20]. In 2D systems, the statistics support the BKT transition as well.

Experiment. Theoretically, no lattice is necessary for the BKT transition. However, observations of optical beams in a homogeneous photorefractive crystal have resulted in condensation only[20]. Reasons for this are unclear, but it may result from the relatively slow growth of instability (especially with defocusing nonlinearity), the related limitation of finite crystal length, or the presence of charge smearing in the electro-optic response that limits the dynamics at small scales (that is, the initial stages of vortex pair creation and unbinding). Regardless, it was found necessary to introduce a lattice potential to observe BKT dynamics.

The experimental set-up is shown in Fig. 2. A finite-size, 10 mW beam is projected onto a spatial light modulator. The spatial light modulator creates a random-phase field with a user-defined correlation length l_c. Nonlinear wave action occurs in a 5 × 5 × 10 mm SBN:75 ($Sr_{0.75}Ba_{0.25}Nb_2O_6$) photorefractive crystal with a coupling strength controlled by applying a voltage across the c axis. A periodic potential is optically induced by interfering plane waves in the crystal (polarized perpendicularly to the c axis)[17], while a separate reference beam (not shown) is split off from the input laser to measure relative phase. This latter beam gives the location and sign of vortices through the characteristic fork pattern of the singularity (Fig. 1b).

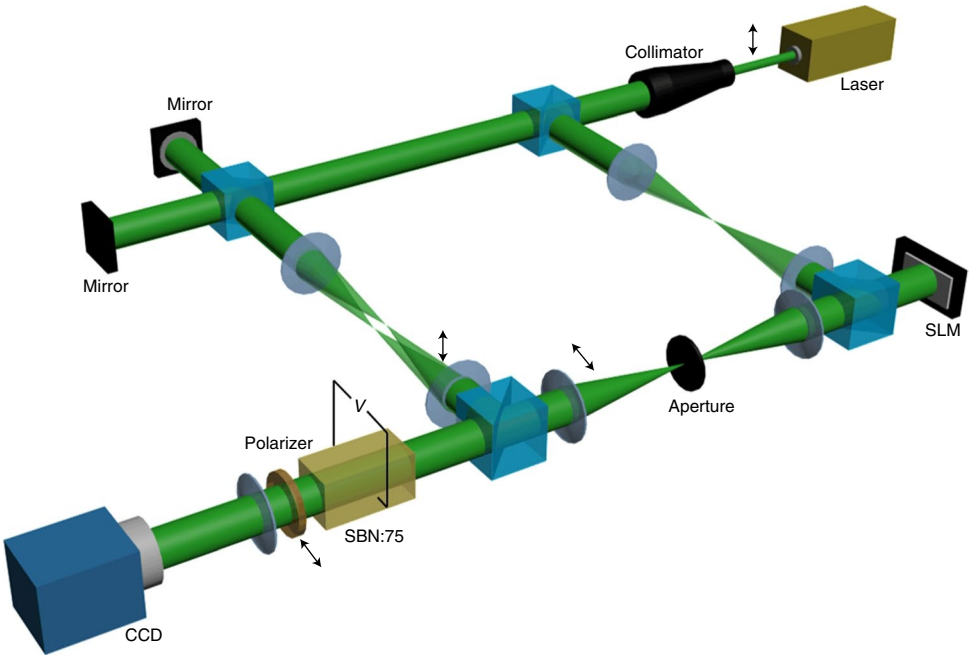

Fig. 2 | Experimental set-up. Light from a 532 nm laser is split into two beams by using a beam splitter. One beam creates an interference grating on a 5 × 5 × 10 mm SBN:75 photorefractive crystal. The other beam acquires a user-controlled random-phase pattern from a spatial light modulator (SLM), which is then imaged onto the input plane of the crystal. The output plane of the crystal is imaged onto the charge-coupled device (CCD) plane and interferes with a tilted reference beam (not shown).

As the desired dynamics are 2D (+ propagation), it is natural to choose a 2D lattice. However, 2D lattices inhibit transport[31–33] at the high nonlinearities needed for vortex formation[14], have different structures when optically induced under focusing or defocusing nonlinearity[17] (complicating comparison), and are prone to instability over the long timescales of the experiment (see Methods for details). To overcome these problems, we used a 1D lattice, that is, a potential periodic in one direction only. This planar array is symmetric under sign changes, more stable than its 2D counterparts, and has a continuity in the transverse direction that encourages smooth vortex flow. Moreover, there is essentially no difference in BKT behaviour in 1+1+1D systems versus 2+1D systems[34]. Indeed, observations of the BKT transition in cold atoms[6] and superconductors[35] have used the planar lattice geometry as well.

Dynamics occur throughout the crystal as the light propagates, but only the output face of the crystal can be imaged. Nevertheless, a 'snapshot' at the propagation distance $z = L_{\mathrm{crystal}}$ (Fig. 1b) clearly shows the main ingredients: (1) many more vortices at the output compared with the input; (2) sets of vortex pairs; and (3) sets of free vortices. The number of free vortices, obtained easily by counting the phase singularities, determines the superfluid properties of the light[15,18].

The statistical dynamics of the system can be characterized by the radial correlation function

$$C(r) = \iint\limits_{r \le \sqrt{x^2+y^2} \le r+\mathrm{d}r} \mathrm{d}x\mathrm{d}y A^*(x_0, y_0) A(x_0 + x, y_0 + y)$$

Below the BKT transition, $C(r)$ obeys a power law (Fig. 3), indicating that the correlations are long-range and scale-free. Above the transition, vortex creation and unbinding destroys coherence, resulting in an exponentially decaying correlation function. The correlation length $\xi(T) \sim \exp\left[B(T - T_c)^{-1/2}\right]$ has the typical $(T - T_c)^{1/2}$ dependence on the critical temperature T_c expected from Ginzburg–Landau theory but with an essential singularity arising from (renormalized) vortex interactions[36]. On average, the correlation length determines the density of vortices in a given area Ω, through $N/\Omega \sim \xi^{-2}$, so that the expected number of vortices is[12,36]

$$N(T) = AH(T - T_c) \exp\left[-2B(T - T_c)^{-1/2}\right] \qquad (6)$$

where $H(T)$ denotes the Heaviside step function and A and B are non-universal fitting parameters related to the integration area (system size). As shown in Fig. 4a,b, the number of new vortices is well matched by the prediction (equation (6)) ($R^2 > 0.995$), with a constant value $A = 5{,}000$ for all cases. The experiments confirm that nonlinear interactions change the transition temperature[4,12], with $T_c = \{0.68, 0.62, 0.58\}$ for applied bias $E_0 = \{-250\ \mathrm{V}, -350\ \mathrm{V}, -450\ \mathrm{V}\}$, and show that the transition is the same for either sign of nonlinearity. In all cases, the number of vortices produced is lower in the self-focusing case, due to enhanced attraction and recombination of vortex pairs.

It proves convenient to express the spatial distribution in terms of the correlation parameter $|A_Q|$, where the radial wavenumber Q is defined through[12,37] $|A_Q|^2 \propto \Omega \int_0^{\sqrt{\Omega}} r|C(r)|^2 \mathrm{d}r$. Above the transition temperature, the exponential decay gives $|A_Q|^2 \propto \Omega$. Below the transition, the field should have quasi-long-range order, with a scale-free correlation function $C(r) \propto r^{-\alpha(T)}$ that gives[36] $|A_Q|^2 \propto \Omega^{2-\alpha}$. Hence, the crossover can be characterized by fitting $|A_Q|$ to $\Omega^{\kappa(T)}$, where $\kappa = 0.5$ above the transition and $\kappa = 0.875$ at the transition temperature T_c ($\alpha_c = 0.25$ as $T \to T_c$ from below)[36,38]. Experimental measurement of this exponent is shown in Fig. 4c,d. It is clear that the correlation functions obey the exact scaling behaviour predicted by BKT theory, but the predicted step function at T_c is replaced by a smooth transition, an effect attributable to the finite size of our system[6,39]. Saturation of the exponent at low temperatures (rather than a continuation to $\kappa = 1$) was observed in ref. [6] as well and remains an outstanding issue. We note that the exponent κ gives the inverse superfluid stiffness, through $2\pi[2 - 2\kappa(T)]$; its change across the

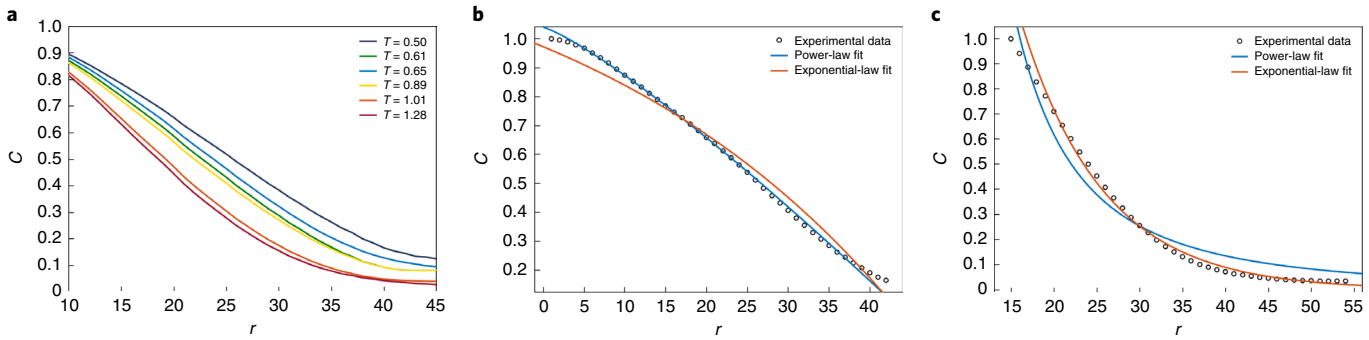

Fig. 3 | Behaviour of the radial correlation function. a, Normalized correlation function of the measured fields as a function of temperature, for a lattice spacing of 10 μm. **b**,**c**, Power-law and exponential fits of the correlations below the transition ($T = 0.5$, $R^2 = 0.99$; **b**) and above the transition ($T = 1.28$, $R^2 = 0.98$; **c**).

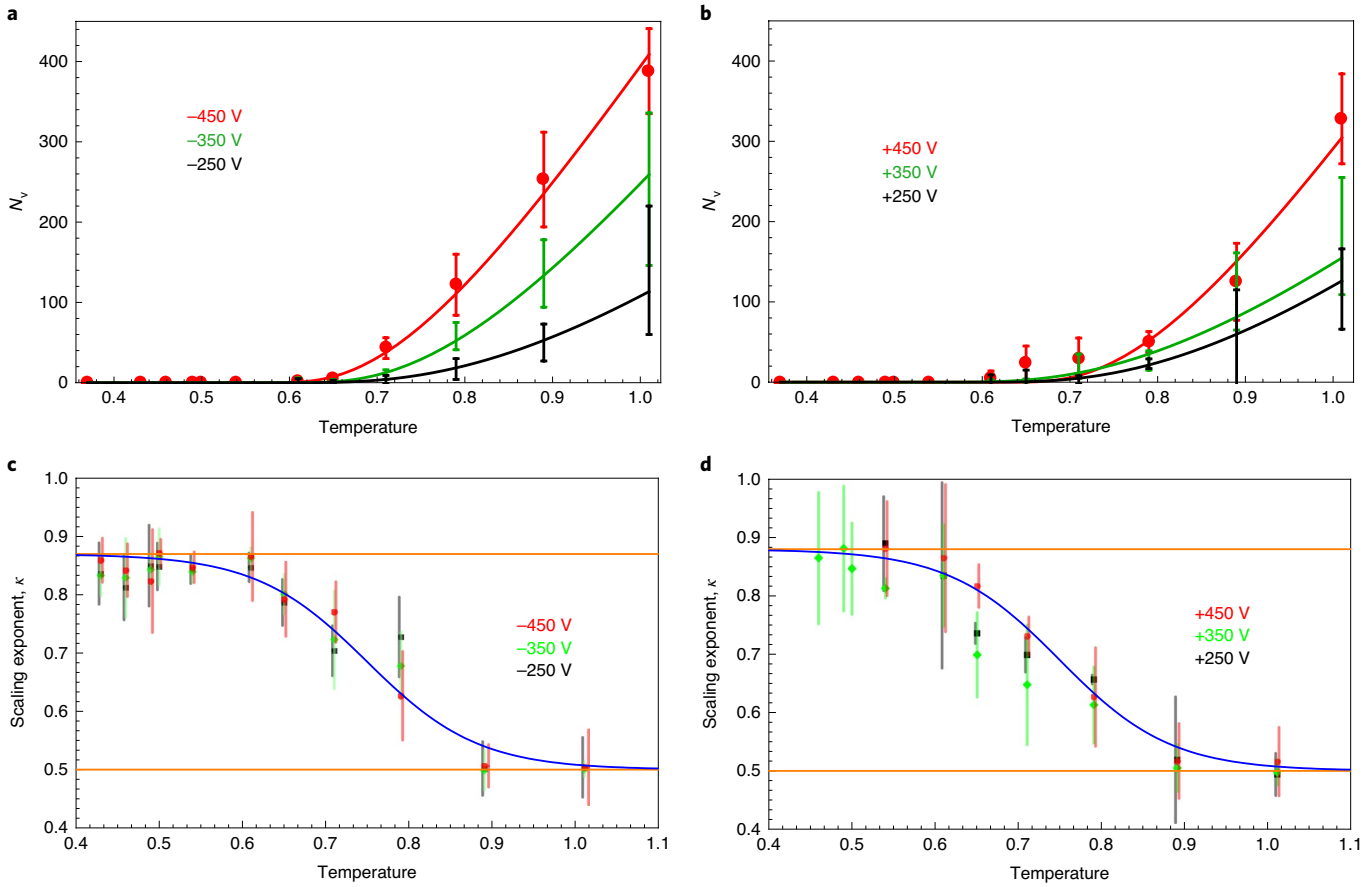

Fig. 4 | Direct measurement of vortex number and correlation function. a,**b**, Number of unbound vortices N_v for self-defocusing (repulsive) (**a**) and self-focusing (attractive) (**b**) nonlinearity, as a function of interaction strength and input temperature, for a lattice spacing of 10 μm. Solid lines indicate predictions from BKT theory. **c**,**d**, Scaling exponent κ versus temperature. When $\kappa = 0.5$, the correlation function undergoes a fast (exponential) decay, while when $\kappa = 0.875$ it decays algebraically. The exponent κ gives the inverse superfluid stiffness through $2\pi[2 - 2\kappa(T)]$. The solid lines are fits to tanh functions[36]. The error bars correspond to the standard deviation.

transition corresponds to a universal jump in density[38]. This jump, which compounds the existing compressibility of the light[18,19], is difficult to observe directly.

The sign of the free energy $F = E - TS$, where S is the entropy, also changes at the transition[4]. We explore an aspect of this here by measuring the transition as a function of lattice spacing. Thermodynamically, smaller lattice spacings give more sites available for occupation (for a fixed area), increasing the entropy and lowering the critical temperature needed to overcome the vortex interaction energy. As shown in Fig. 5a, we observe a linear relationship between the lattice period and T_c. Interestingly, there is a finite transition temperature as the lattice spacing → 0. In this limit, long-wavelength thermal excitations see a potential that is effectively uniform, reducing the dynamics to that of a homogeneous system. Experiments in this regime reveal only wave condensation, with no evidence of vortex production[20].

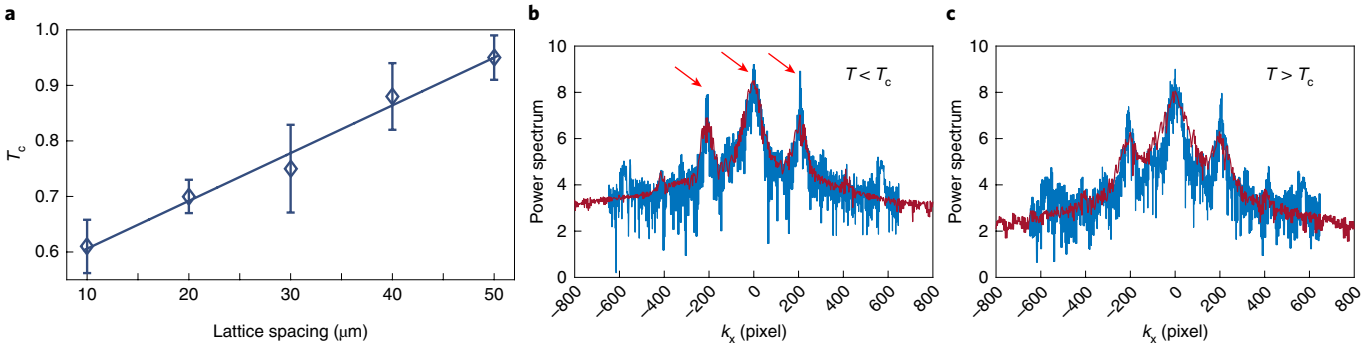

Fig. 5 | Lattice behaviour of the photonic BKT transition. a, Critical temperature for vortex production as a function of lattice period. For fixed potential well depth (constant coupling between sites), different lattice spacings correspond to different dominant wavelengths of instability. **b**,**c**, Power spectra, in terms of the transverse wavenumber k_x, for a lattice spacing of 10 μm and applied voltage of −350 V. Condensation spikes at $k_x = 0$ and $k_x = \pm k_B$ before the transition (shown by red arrows, **b**) diminish or disappear after the transition (**c**). Blue, experiment; brown, simulation. The error bars correspond to the standard deviation.

The signature of condensation is a sharp peak at the lowest-available mode (for example, $k = 0$)[20]. In a lattice system, peaks also occur at the edges of the Brillouin zones (clear from either standing-wave reinforcement or diffraction orders in the periodic grating)[40]. These features in the power spectra are shown in Fig. 5b,c. Note that the peak at $k = 0$ is completely eliminated but the ones at $k = \pm k_B$ (where $k_B = \pi/d$ is the Bragg angle, with d the lattice period) are only reduced, as some condensate remains trapped in the potential wells and there is still transverse, counter-propagating flow within the vortices.

Discussion

The lattice potential introduces four dynamical elements that are not present in homogeneous systems. First, the periodicity breaks the phase-matching condition of four-wave mixing, suppressing the cascade mechanism of condensate formation[41]. Second, the lattice provides sites for the nucleation of vortices. Third, the band structure modifies the dispersion (diffraction) relation, changing the effective mass of the photons and altering the stiffness[42] and nonlinear response[17] of the corresponding fluid. And fourth, the lattice provides a competing periodicity once perturbations arise, facilitating supercontinuum generation[43] and the breakup of ordered states[44].

In the planar lattice geometry studied here, there is an interesting competition between discrete and continuous dynamics. Discrete models (for example, *XY*) ignore smooth fields and fluid degrees of freedom, while continuous models (for example, wave turbulence) have trouble accommodating vortices, both because they are singular structures and because they are not weak perturbations[14]. Nevertheless, each viewpoint provides an independent, self-consistent description of the transition.

From the fluid viewpoint, the periodic potential provides a series of boundaries that refract the flow. At each interface, changes in angular momentum in the beam create modulations and vorticity (Fig. 6a). The lattice also dephases emitted density (sound) waves, preventing their reabsorption by the perturbation and further destabilizing the wave (for example, by encouraging snaking)[45]. Larger separation distance between vortex pairs corresponds to weaker interaction strength and thus a weaker instability. More kinetic energy is required to overcome the decrease, leading to larger critical temperatures for the transition (Fig. 4a).

From the discrete viewpoint, the periodic potential provides transmission bands whose curvature determines spatial transport[40] (Fig. 6b). Bragg reflections create regions of differing curvature (positive or negative), enabling the system to support the transition with either focusing or defocusing nonlinearity. Either

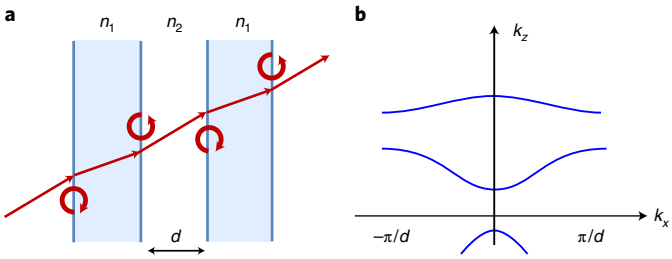

Fig. 6 | Interpretations of lattice dynamics. a,**b**, The induced lattice can be interpreted as a series of boundaries (**a**) or a periodic potential with transmission bands (**b**). **a**, Optical flow refracts at each interface, changing the angular momentum and generating vorticity. **b**, Bragg reflections cause π phase shifts at the ends of each Brillouin zone, seeding vortices. Spatial dynamics and nonlinear response are determined by band curvature. Both viewpoints support vortex–antivortex pair formation for either sign of nonlinearity. n_i, indices of refraction; d, lattice spacing.

way, counter-streaming waves lead to π phase changes at adjacent sites, laying the foundation for vortex solitons[32]. However, forming these vortices becomes more difficult with larger lattices: longer periods stretch out initial perturbations, making it easier for oscillations to heal to the spacing of the lattice. As before, weaker growth requires a greater critical energy to incite and subsequently disorder the vortices.

In photonics, coherence and vortex dynamics are normally considered separately, with emission and lasing on one hand and angular momentum modes on the other. In 2D systems, however, there is a complex relationship between them. These effects arise naturally on surfaces and will become increasingly important as 2D devices are engineered[46–48]. As in traditional fluids, the coupling of vortices with intensity/pressure variations is fundamental to transport, instability and long-range order. The results here give a thermodynamic endpoint to these studies, as well as a starting point for exploring the full phase space of non-equilibrium and vortex-coherence dynamics.

Online content

Any methods, additional references, Nature Research reporting summaries, source data, extended data, supplementary information, acknowledgements, peer review information; details of author contributions and competing interests; and statements of data and code availability are available at https://doi.org/10.1038/s41566-020-0636-7.

Received: 8 January 2018; Accepted: 7 April 2020;
Published online: 13 July 2020

References

1. Hohenberg, P. C. Existence of long-range order in one and two dimensions. *Phys. Rev.* **158**, 383–386 (1967).
2. Mermin, N. D. & Wagner, H. Absence of ferromagnetism or antiferromagnetism in one- or two-dimensional isotropic Heisenberg models. *Phys. Rev. Lett.* **17**, 1133–1136 (1977).
3. Berezinskii, V. L. Destruction of long-range order in one-dimensional and two-dimensional systems having a continuous symmetry group 1. Classical systems. *Sov. Phys. JETP USSR* **32**, 493–500 (1971).
4. Kosterlitz, J. M. & Thouless, D. J. Ordering, metastability and phase transitions in two-dimensional systems. *J. Phys. C* **6**, 1181–1203 (1973).
5. Ketterle, W. & van Druten, N. J. Bose-Einstein condensation of a finite number of particles trapped in one or three dimensions. *Phys. Rev. A* **54**, 656–660 (1996).
6. Hadzibabic, Z., Krueger, P., Cheneau, M., Battelier, B. & Dalibard, J. Berezinskii–Kosterlitz–Thouless crossover in a trapped atomic gas. *Nature* **44**, 1118–1121 (2006).
7. Bishop, D. J. & Reppy, J. D. Study of the superfluid transition in two-dimensional ^{4}He films. *Phys. Rev. Lett.* **40**, 1727–1730 (1978).
8. Resnick, D. J., Garland, J. C., Boyd, J. T., Shoemaker, S. & Newrock, R. S. Kosterlitz-Thouless transition in proximity-coupled superconducting arrays. *Phys. Rev. Lett.* **47**, 1542–1545 (1981).
9. Roumpos, G. et al. Power-law decay of the spatial correlation function in exciton-polariton condensates. *Proc. Natl Acad. Sci. USA* **109**, 6467–6472 (2012).
10. Aranson, I. S., Chaté, H. & Tang, L.-H. Spiral motion in a noisy complex Ginzburg-Landau equation. *Phys. Rev. Lett.* **80**, 2646–2649 (1998).
11. Huepe, C., Riecke, H., Daniels, K. E. & Bodenschatz, E. Statistics of defect trajectories in spatio-temporal chaos in inclined layer convection and the complex Ginzburg–Landau equation. *Chaos* **14**, 864–874 (2004).
12. Small, E., Pugatch, R. & Silberberg, Y. Berezinskii-Kosterlitz-Thouless crossover in a photonic lattice. *Phys. Rev. A* **83**, 013806 (2011).
13. Dagvadorj, G. et al. Nonequilibrium phase transition in a two-dimensional driven open quantum system. *Phys. Rev. X* **5**, 041028 (2015).
14. Nazarenko, S., Onorato, M. & Proment, D. Bose-Einstein condensation and Berezinskii-Kosterlitz-Thouless transition in the two-dimensional nonlinear Schrödinger model. *Phys. Rev. A* **90**, 013624 (2014).
15. Carusotto, I. Quantum fluids of light. *Rev. Mod. Phys.* **85**, 299–366 (2013).
16. Sun, C., Waller, L., Dylov, D. V. & Fleischer, J. W. Spectral dynamics of spatially incoherent modulation instability. *Phys. Rev. Lett.* **108**, 263902 (2012).
17. Fleischer, J. W., Segev, M., Efremidis, N. K. & Christodoulides, D. N. Observation of two-dimensional discrete solitons in optically induced nonlinear photonic lattices. *Nature* **422**, 147–150 (2003).
18. Wan, W., Jia, S. & Fleischer, J. W. Dispersive superfluid-like shock waves in nonlinear optics. *Nat. Phys.* **3**, 46–51 (2007).
19. Jia, S., Haataja, M. & Fleischer, J. W. Rayleigh–Taylor instability in nonlinear Schrödinger flow. *New. J. Phys.* **14**, 075009 (2012).
20. Sun, C. et al. Observation of the kinetic condensation of classical waves. *Nat. Phys.* **8**, 471–475 (2012).
21. Klaers, J., Vewinger, F. & Weitz, M. Thermalization of a two-dimensional photonic gas in a 'white wall' photon box. *Nat. Phys.* **6**, 512–515 (2010).
22. Šantić, N. et al. Nonequilibrium precondensation of classical waves in two dimensions propagating through atomic vapors. *Phys. Rev. Lett.* **120**, 055301 (2018).
23. Klaers, J., Schmitt, J., Vewinger, F. & Weitz, M. Bose-Einstein condensation of photons in an optical microcavity. *Nature* **468**, 545–548 (2010).
24. Aranson, I. S. & Kramer, L. The world of the complex Ginzburg-Landau equation. *Rev. Mod. Phys.* **74**, 99–143 (2002).
25. Coullet, P., Gil, L. & Rocca, F. Optical vortices. *Opt. Commun.* **73**, 403–408 (1989).
26. Gibson, C. J., Yao, A. M. & Oppo, G.-L. Optical rogue waves in vortex turbulence. *Phys. Rev. Lett.* **116**, 043903 (2016).
27. Christodoulides, D. N. & Joseph, R. I. Discrete self-focusing in nonlinear arrays of coupled waveguides. *Opt. Lett.* **13**, 794–796 (1988).
28. Rasmussen, K. Ø., Cretegny, T., Kevrekidis, P. G. & Grønbech-Jensen, N. Statistical mechanics of a discrete nonlinear system. *Phys. Rev. Lett.* **84**, 3740–3743 (2000).
29. Silberberg, Y., Lahini, Y., Bromberg, Y., Small, E. & Morandotti, R. Universal correlations in a nonlinear periodic 1D system. *Phys. Rev. Lett.* **102**, 233904 (2009).
30. Rumpf, B. Transition behavior of the discrete nonlinear Schrödinger equation. *Phys. Rev. E* **77**, 036606 (2008).
31. Lopes, R. J. C. & Moura, A. R. Possible extinction of Berezinskii–Kosterlitz–Thouless transition by diagonal interactions in the checkerboard lattice. *Phys. Lett. A* **382**, 1492–1498 (2018).
32. Fleischer, J. W. et al. Observation of vortex-ring "discrete" solitons in 2D photonic lattices. *Phys. Rev. Lett.* **92**, 123904 (2004).
33. Michel, C., Boughdad, O., Albert, M., Larré, P.-É. & Bellec, M. Superfluid motion and drag-force cancellation in a fluid of light. *Nat. Commun.* **9**, 2108 (2018).
34. Trombettoni, A., Smerzi, A. & Sodano, P. Observable signature of the Berezinskii–Kosterlitz–Thouless transition in a planar lattice of Bose–Einstein condensates. *New J. Phys.* **7**, 57 (2005).
35. Mizukami, Y. et al. Extremely strong-coupling superconductivity in artificial two-dimensional Kondo lattices. *Nat. Phys.* **7**, 849–853 (2011).
36. Chaikin, P. R. & Lubensky, T. C. *Principles of Condensed Matter Physics* (Cambridge Univ. Press, 1995).
37. Polkovnikov, A., Altman, E. & Demler, E. Interference between independent fluctuating condensates. *Proc. Natl Acad. Sci. USA* **103**, 6125–6129 (2006).
38. Nelson, D. R. & Kosterlitz, J. M. Universal jump in the superfluid density of two-dimensional superfluids. *Phys. Rev. Lett.* **39**, 1201–1204 (1977).
39. Bramwell, S. T. & Holdsworth, P. C. W. Magnetization: a characteristic of the Kosterlitz-Thouless-Berezinskii transition. *Phys. Rev. B* **49**, 8811–8814 (1994).
40. Fleischer, J. W. et al. Spatial photonics in nonlinear waveguide arrays. *Opt. Express* **13**, 1780–1796 (2005).
41. Pushkarev, A. N. & Zakharov, V. E. Turbulence of capillary waves—theory and numerical simulation. *Physica D* **135**, 98–116 (2000).
42. Chiao, R. Y. & Boyce, J. Bogoliubov dispersion relation and the possibility of superfluidity for weakly interacting photons in a two-dimensional photon fluid. *Phys. Rev. A* **60**, 4114–4121 (1999).
43. Jia, S., Wan, W. & Fleischer, J. W. Forward four-wave mixing with defocusing nonlinearity. *Opt. Lett.* **32**, 1668–1670 (2007).
44. Guillamon, I. et al. Enhancement of long-range correlations in a 2D vortex lattice by an incommensurate 1D disorder potential. *Nat. Phys.* **10**, 851–856 (2014).
45. Parker, N. G., Proukakis, N. P., Barenghi, C. F. & Adams, C. S. Dynamical instability of a dark soliton in a quasi-one-dimensional Bose–Einstein condensate perturbed by an optical lattice. *J. Phys. B* **37**, S175–S185 (2004).
46. Iga, K. Surface-emitting laser—its birth and generation of new optoelectronics field. *IEEE J. Sel. Top. Quantum Electron.* **6**, 1201–1215 (2000).
47. Xia, F., Wang, H., Dubey, M. & Ramasubramanian, A. Two-dimensional material nanophotonics. *Nat. Photon.* **8**, 899–907 (2014).
48. Rivera, N., Kaminer, I., Zhen, B., Joannopoulos, J. D. & Soljacic, M. Shrinking light to allow forbidden transitions on the atomic scale. *Science* **353**, 263–269 (2016).

Methods

The temperature is defined in relation to the correlation of the initial phase field. More specifically, this function decays exponentially with a $(1/e)$ width ξ, allowing the temperature T to be defined as[12]

$$T = \frac{1}{a\xi + 1/\tilde{T}}$$

Here $a = 0.07$ and $\tilde{T} = 1.76$ is the maximum temperature that can be achieved with phase-only fluctuation.

Phase measurements of the input and output faces of the crystal were made by interfering these beams with a tilted reference beam. Vortices were then identified by the characteristic fork patterns of their phase singularities. The length scale for vortices is given by the width of their (dark) cores. We define bound vortices by pairs that are separated by three core lengths or less.

As described in the Discussion, the formation of vortex–antivortex pairs results from instabilities in the propagating beam. Ideally, these are triggered by noise (temperature fluctuations) in the homogeneous system; here they are seeded by both noise and the lattice. At the maximum applied voltage of ±450 V, the nonlinear index change is measured to be $|\Delta n/n_0| = 6\times 10^{-4}$. For vortices that are already well developed, this nonlinearity is strong enough to pin them to lattice sites (for example, via 2D vortex lattice solitons[32]). However, the formation of vortex–antivortex pairs from (cascaded) instability is very slow at this strength: the development of the dynamics to steady state (necessary to assure the validity of the beam propagation model (equations (1) and (2)) was approximately tens of minutes. This timescale is one to two orders of magnitude slower than previous lattice experiments in photorefractives (including those where the lattice itself moved, for example phason shifts[49] and rotating arrays for artificial gauge fields[50]). Optically induced lattices in photorefractive media are more phase-sensitive in two dimensions than in one dimension and, in practice, mechanical vibrations of the mirror mounts and environmental fluctuations in the lab prevented the use of 2D geometry.

Captured images are 1,216 × 1,616 pixels, with pixel size 0.55 × 0.55 μm^2. The lattice period in our experiments (except Fig. 5a) was 10 μm. Each data point in Figs. 3–5 represents an ensemble average of 10 different representations of the experiment (10 different samples from the initial temperature distribution). The error bars correspond to the standard deviation of these measurements.

Simulations for Fig. 5b,c were performed using a standard (2+1)D Fourier split-step beam propagation code. Periodic boundary conditions were chosen, with the lattice modelled as a continuous, sinusoidal potential. More details can be found in the Supplementary Information.

Data availability

The data that support the plots within this paper and other findings of this study are available from the corresponding authors upon reasonable request. Source data are provided with this paper.

References

49. Freedman, B. et al. Wave and defect dynamics in nonlinear photonic quasicrystals. *Nature* **440**, 1166–1169 (2006).
50. Jia, S. & Fleischer, J. W. Nonlinear light propagation in rotating waveguide arrays. *Phys. Rev. A* **79**, 041804(R) (2009).

Acknowledgements

This work was supported by the Air Force Office of Scientific Research (grants FA9550-12-1-0054 and FA9550-14-1-0177), the Chinese Academy of Sciences (grant QYZDB-SSW-JSC002) and Sino-German Center for Sino-German Cooperation Group (grant GZ 1391).

Author contributions

G.S. and J.W.F. conceived and designed the experiments. G.S. performed the experiments and simulations. G.S. and J.W.F. analysed the data and contributed to the preparation of the manuscript.

Competing interests

The authors declare no competing interests.

Additional information

Supplementary information is available for this paper at https://doi.org/10.1038/s41566-020-0636-7.

Correspondence and requests for materials should be addressed to G.S. or J.W.F.

Reprints and permissions information is available at www.nature.com/reprints.